ADVANCED OPTICAL MATERIALS
www.advopticalmat.de

# Visible-Light-Actuated Bidirectional Photochromism in Chiral Nanostructures with Multi-Degree of Freedom

*Xiaojun Liu, Dashuai Liu, Yuxuan Cheng, Lang Qin,* and Yanlei Yu*

**Cholesteric liquid crystals (CLCs) with chiral nanostructures take on great significance in light modulation for optical devices, especially involving the features of circularly polarized and dynamic structural colors. However, on-demand self-assembly by photoprogramming still remains a challenge that is ascribed to the unpredictable variation of the helical superstructures in the existing CLCs induced by light-driven chiral switches. Here, novel binary chiral systems are designed to construct visible-light-actuated CLCs with multi-degrees of freedom, including adjustable circular polarization, bidirectional photochromism, and manipulable photonic bands. Such systems consist of an *o*-fluoroazobenzene-containing chiral switch and an inert chiral dopant, whose interaction dominates the strategies of chiral cooperation or conflict to determine the CLC handedness as well as shift direction of the selective reflection. Particularly, the precise tuning range of the structural color is tailored by programmable helical twisting power to enable diverse paradigms of light-actuated patterning. The unprecedented quantitative manipulation of circularly polarized structural colors offers unique photonic attributes for applications in information encoding and multiplexed communication.**

## 1. Introduction

Hierarchical chiral nanostructures present in living systems exhibit distinctive chiroptical properties, enabling selective interaction with light of specific polarization states to manipulate visual appearance for courtship, predation, and camouflage.[1–3] For example, the renowned jewel beetle *Chrysina gloriosa* has been discovered to only reflect left-handed circularly polarized light, resulting in a brilliant green metallic iridescence that arises from the helicoidally stacked chitin nanofibrils and the mosaic of cusps containing focal conic domains with a left-handed helix.[4] Recently, another beetle species called *Chrysina resplendens* was observed to reflect both left- and right-handed circularly polarized light due to its sophisticated helicoidal architecture within the cuticle. This architecture comprises two layers of left-handed helicoids sandwiching an intermediate layer as a half-wave retardation plate.[5] Inspired by these hierarchical chiral nanostructures, significant efforts have been devoted to fabricating optical materials capable of modulating the polarization of light,[6–9] which paves the way for applications in displays,[10–15] color filters,[16] and anti-counterfeiting technologies.[17–21]

Cholesteric liquid crystal (CLC) is a promising candidate for mimicking the chiral nanostructures in nature, where the self-assembly of liquid crystal (LC) mesogens results in periodic helical superstructures with a specific rotation direction along the perpendicular axis.[22–25] This periodic helical superstructure creates a photonic bandgap that selectively reflects light with the same handedness while transmitting light with the opposite handedness as the CLC, thereby demonstrating structural coloration through circularly polarized reflection (CPR).[26–32] Light-actuated CLCs are currently at the forefront of research due to their exceptional dynamic tunability upon external stimuli, particularly leveraging the advantages of remote, spatial, and temporal controllability offered by light.[33–36] Such elegant nanostructures are typically fabricated by doping miscible light-driven chiral switches into achiral nematic LCs,[37] whose steric configuration determines the handedness of the CLC (helicity) and the ability to twist the LC mesogens (helical twisting power, HTP, $\beta$).[38–41] Upon light irradiation, the chiral switches undergo photoisomerization, leading to changes in configurations, HTP values, and even helicity, which subsequently allows for manipulation of reflection wavelength and polarization.[42] The most popular photoresponsive groups for designing chiral switches include azobenzenes, diarylethenes, and molecular motors.[43] The *trans*-to-*cis* photoisomerization of azobenzene results in a structural transformation of the chiral switch from rod-like to bent shape, which contributes to the large variation of the HTP value and CPR.[44,45] Diarylethene undergoes open-close ring isomerization with limited geometric change, exhibiting remarkable thermal stability but restricted HTP variation.[46–48] The molecular motors confer convertible CPR to CLCs through drastic configurational transformations between distinct isomeric states, therefore enabling the creation of colorful patterns that demonstrate both left- and right-handed CPR under local illumination.[49,50] Although the light-directed

X. Liu, D. Liu, Y. Cheng, L. Qin, Y. Yu
Department of Materials Science and State Key Laboratory of Molecular Engineering of Polymers
Fudan University
Shanghai 200433, P. R. China
E-mail: qinlang@fudan.edu.cn

The ORCID identification number(s) for the author(s) of this article can be found under https://doi.org/10.1002/adom.202402177

**DOI: 10.1002/adom.202402177**

 

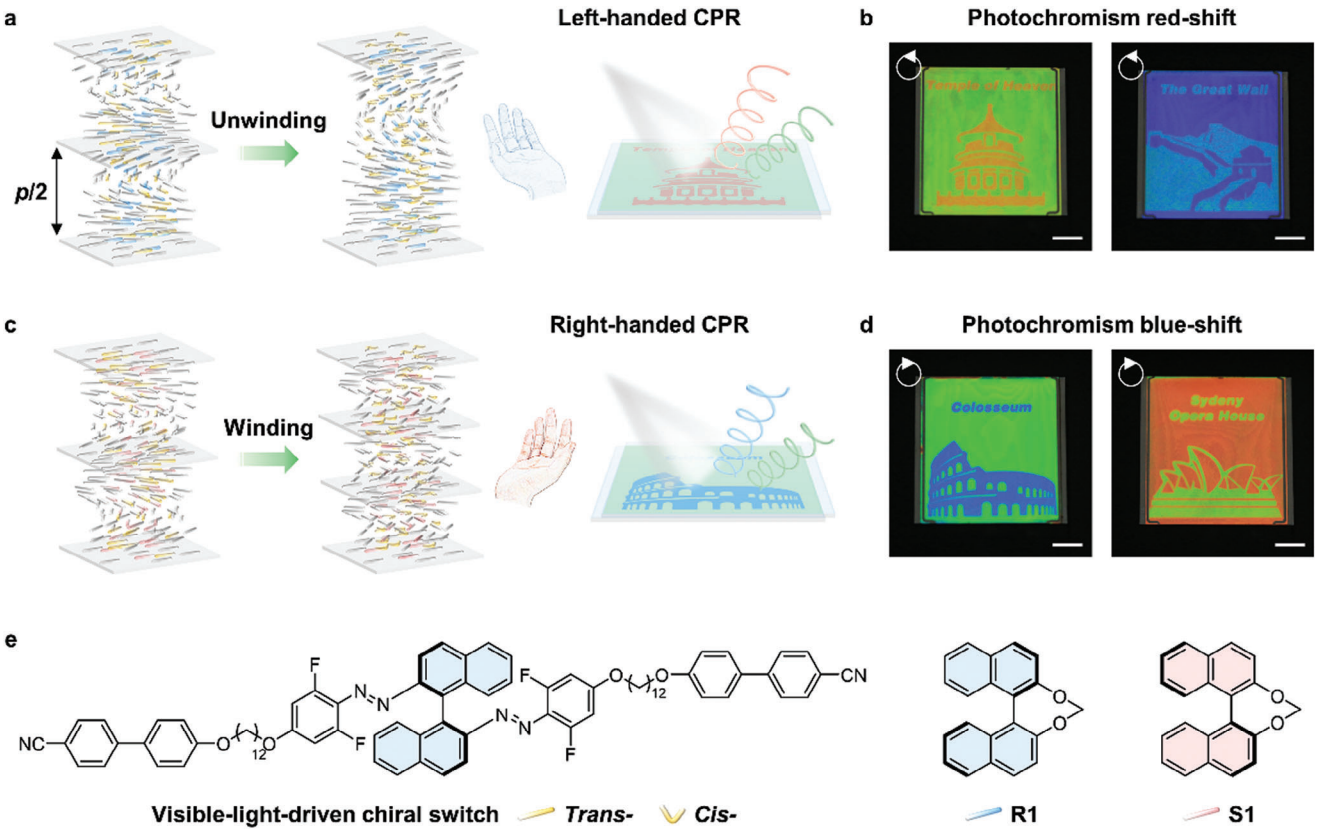


**Figure 1.** a) Schematic illustration to show the unwinding of the chiral nanostructures that exhibit structural coloration with left-handed circularly polarized reflection (CPR). *p*, the pitch length of the cholesteric liquid crystals (CLCs). b) Photographs to show the photochromic patterns (left: *Temple of Heaven*, right: *The Great Wall*) of the CLCs constructed by visible-light-actuated redshift. Scale bar, 1 cm. c) Schematic illustration to show the winding of the chiral nanostructures that exhibit structural coloration with right-handed CPR. d) Photographs to show the photochromic patterns (left: *Colosseum*, right: *Sydney Opera House*) of the CLCs constructed by visible-light-actuated blue-shift. Scale bar, 1 cm. e) Chemical structures of the newly-designed visible-light-driven chiral switch, chiral dopants R1 and S1.

precise variation of RGB structural colors via photochemical phase transition of CLC system[44] or diverse photostationary states[51] have been realized in our previous research, the tuning of polarization and shift direction of the reflection wavelength is still uncontrollable. The helical superstructures still encounter significant challenges in on-demand self-assembly by photoprogramming (e.g., shift direction and tuning range of specific CPR) due to the unpredictable variation of HTP values. Additionally, there is a strong preference for visible-light-actuated CLCs in order to avoid material degradation and enhance device longevity by moving away from high-energy UV light.[51]

Herein, visible-light-actuated CLCs with multi-degree of freedom (DOF), including adjustable circular polarization, bidirectional photochromism, and manipulable photonic bands are constructed by newly-designed binary chiral systems that consist of an *o*-fluoroazobenzene-containing chiral switch and an inert chiral dopant (**Figure 1**). The binary chiral systems satisfy simultaneously on-demand manipulation of the overall handedness and HTP variation in a quantitative manner, achieved through strategies of chiral cooperation or conflict. Interestingly, based on these principles, we demonstrate the synchronous tuning of double-layer CLCs with programmable photochromic properties to extract or conceal visible-light-actuated patterns featuring opposite CPR, thus showing potential applications in optical multiplexing and anti-counterfeiting technologies.

## 2. Results and Discussion

The chiral nanostructures with multi-DOF were designed according to three criteria: 1) the CLCs must be actuated by visible light; 2) the self-assembly of helical superstructures must be programmable to control the polarization and shift direction of the reflection wavelength; and 3) the dynamic tuning range of the structural color must be manipulable. The first requirement is satisfied by designing a fluorinated chiral switch (Figure 1e; Figure S1, Supporting Information), where the n-$\pi*$ bands of the *trans* and *cis* isomers are separated by the introduction of fluorine atoms *ortho* to the azo moiety.[52] The *ortho*-fluorine atoms reduce the electron density in the neighboring N=N bond and thus lower the n-orbital energy, allowing for selective excitation of the two isomers in the visible spectrum (green and blue light).[53–55] To satisfy the second criterion, strategies based on chiral cooperation and conflict are employed to construct the binary chiral systems composed of the visible-light-driven chiral switch and chiral dopants (R1 and S1, Figure S2, Supporting Information) that possess different configurations. In this scenario, the

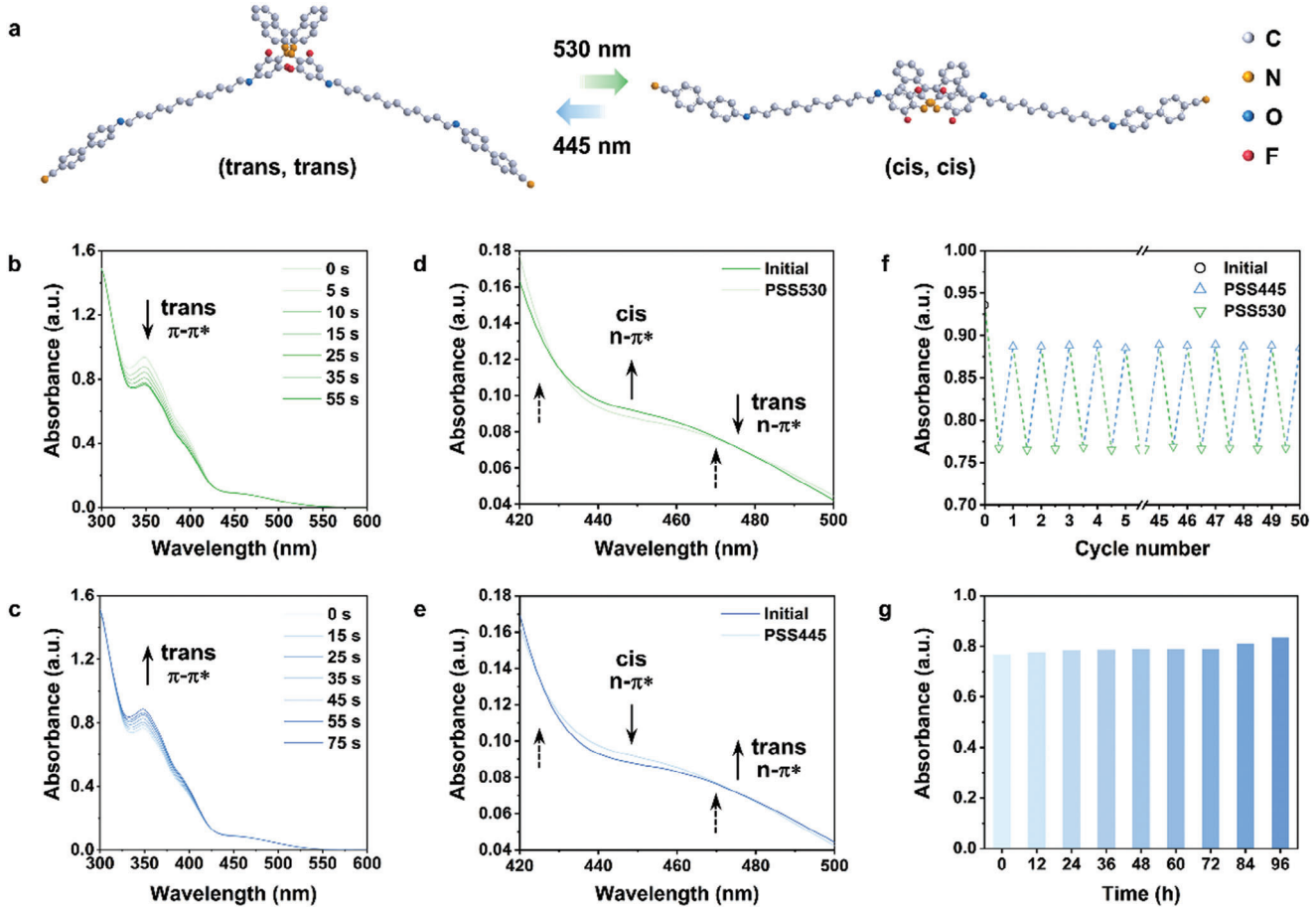


**Figure 2.** a) Optimized molecular structures of the visible-light-driven chiral switch in (*trans*, *trans*) and (*cis*, *cis*) configurations. Hydrogen atoms are omitted for clarity. b,c) Absorption of the chiral switch in dichloromethane ($2.5 \times 10^{-5}$ M) upon b) 530 nm light (30 mW cm$^{-2}$) and c) 445 nm light 25 mW cm$^{-2}$). d,e) Enlarged UV–vis spectra in the visible region (420–500 nm) of the chiral switch in dichloromethane ($2.5 \times 10^{-5}$ M) upon d) 530 nm light (30 mW cm$^{-2}$) and e) 445 nm light (25 mW cm$^{-2}$). The dotted arrows denote two isosbestic points at 425 and 470 nm. PSS, photostationary state. f) Fatigue resistance of the chiral switch in dichloromethane ($2.5 \times 10^{-5}$ M) upon exposure to alternating 530 nm light (30 mW cm$^{-2}$) and 445 nm light (25 mW cm$^{-2}$). g) Thermal stability of the chiral switch at the $PSS_{530}$ in dichloromethane ($2.5 \times 10^{-5}$ M). The intensity variation of the $\pi$–$\pi*$ absorption band at 348 nm is recorded.

different chirality of the CLCs dominated by the chiral dopants will give rise to opposite HTP variation after photoisomerization of the chiral switch, which notably demonstrates bidirectional photochromism, i.e., red and blueshift of the reflection wavelength, in the CLCs. Moreover, the last requirement is satisfied by precisely manipulating the overall HTP values of the binary chiral systems according to the theoretical equations.

The visible-light-driven chiral switch was synthesized according to a facile route (Figure S1, Supporting Information). The binaphthalene as an axially chiral center endows the chiral switch with a high initial HTP value.[56] The fluoroazobenzene photoswitches near the binaphthalene chiral center reversibly isomerize between rod-like *trans* form and bent *cis* form upon visible light irradiation, which contributes to significant changes in the steric (*trans*, *trans*) and (*cis*, *cis*) configurations (**Figure 2a**). The introduction of rigid mesogenic cores (4-cyanobiphenyl) and flexible alkyl chains ($-C_{12}H_{24}-$) increases the solubility of the chiral switch in the LC host.

The visible-light-driven photoisomerization of the chiral switch was comprehensively investigated by UV–vis spectra upon exposure to 530 and 445 nm light. As shown in Figure 2b,c, the 530 nm light induces *trans-cis* isomerization while the 445 nm light triggers the reverse *cis-trans* back process, which is evidenced by the intensity decrease and increase of the $\pi$–$\pi*$ absorption band at 348 nm of the *trans* isomers, respectively. To gain further insight into the visible region of the enlarged spectra (420–500 nm, Figure 2d,e), two isosbestic points at 425 and 470 nm appear due to the separation of the n-$\pi*$ absorption bands of the two isomers. The maximum n-$\pi*$ absorption band of the *cis* isomers (448 nm) blueshifts 28 nm compared to that of the *trans* isomers (476 nm), ascribing to the substitution of electron-withdrawing fluorine atoms. The visible-light-driven chiral switch realized robust fatigue resistance and performed inconspicuous degradation after 50 cycles of sequential exposure to 530 and 445 nm light (Figure 2f). Furthermore, such a chiral switch exhibited negligible intensity variation of the $\pi$–$\pi*$ absorption band at 348 nm after 90 h, which presented excellent thermal stability owing to

the thermally stable *cis* isomers of the fluoroazobenzene with a remarkably long half-life (Figure 2g).[57] As demonstrated, the fluoroazobenzene is a key building block to endow the chiral switch with visible-light-response performance, fatigue resistance, and thermal stability, which are highly desirable for manipulating dynamic selective reflection and pitch length in the CLCs.

When a small amount of the visible-light-driven chiral switch was doped into the commercial LC host E7, an optically tunable cholesteric phase with left-handedness was induced (Figure S3, Supporting Information). The characteristic fingerprint texture in a 5 μm thick homeotropic aligned cell was observed by a polarized optical microscope at a low concentration of 0.2 mol% (Figure S4, Supporting Information). The helical superstructures disappeared upon 530 nm light irradiation, testified by the conoscopic textures, because of the HTP value decrease. The reverse process (i.e., the appearance of fingerprint texture) occurred upon light irradiation at 445 nm. The HTP at the initial state and photostationary states (PSS) was measured by using wedge cells according to the Grandjean-Cano method (Figure S5, Supporting Information).[58] The chiral switch exhibited −85 $\mu m^{-1}$, mol% at the initial state and a considerable 78% HTP difference at the $PSS_{530}$ (−18 $\mu m^{-1}$, mol%), which resulted from the configurational changes during photoisomerization. Upon subsequent exposure to 445 nm light, the HTP value recovered to −43 $\mu m^{-1}$, mol% (Figure S6, Supporting Information). However, the visible-light-driven chiral switch has specific chirality and fixed variation of the HTP values, which is inadequate for multi-DOF photoprogramming of the chiral nanostructures. Therefore, we prepared binary chiral systems based on the concept of conflict and cooperation by combining the chiral dopants that dominate the overall handedness. As depicted in **Figure 3a**, when the helical twisting sense of the dopant S1 (right-handedness) is different from that of the chiral switch (Figure S3, Supporting Information), the helical superstructures wind more tightly upon 530 nm light irradiation since the *cis*-isomer of the chiral switch exhibits weakened HTP compared to that of the *trans*-isomer. In contrast, when the chirality of the dopant R1 (left-handedness) is the same as the chiral switch, light irradiation at 530 nm still decreases the overall HTP of the system (Figure 3b). It is noted that these two systems arising from the chiral conflict or cooperation demonstrate overall different handedness as well as the opposite direction of the HTP variation, serving as ideal candidates for bidirectional photochromism in the CLCs.

Furthermore, another advantage of the binary chiral system lies in the manipulable dynamic range of the HTP values, which directly determine the photochromic properties of the self-assembly helical superstructures. The HTP values ($\beta$) and the tuning range ($\Delta\beta$) of the binary chiral systems follow the equations:

$$\beta_0 = -85w_1 + \beta_d \cdot w_2 \tag{1}$$

$$\beta_{PSS530} = -18w_1 + \beta_d \cdot w_2 \tag{2}$$

$$\Delta\beta = \beta_{PSS530} - \beta_0 = 67w_1 \tag{3}$$

$$w_1 = \frac{c_1}{c_1 + c_2} \tag{4}$$

$$w_1 + w_2 = 100\% \tag{5}$$

where $\beta_0$ and $\beta_{PSS530}$ are the HTP values of the binary chiral systems at the initial state and $PSS_{530}$. $\beta_d$ represents the HTP values of the chiral dopants, where the values of both S1 and R1 are the same but with opposite sense. For S1, $\beta_d$ is 57 $\mu m^{-1}$ (mol%), while $\beta_d$ is −57 $\mu m^{-1}$ (mol%) for R1 (Figure S7, Supporting Information). ($w_1$, $w_2$) and ($c_1$, $c_2$) denote the ratios and the molar concentration percentages of the visible-light-driven chiral switch and chiral dopants (S1 or R1), respectively. Most importantly, the ratio of the chiral switch $w_1$ determines the manipulation of the initial HTP values and the tuning range according to Equations (1) and (3). The initial HTP values decrease while the tuning range increases as $w_1$ increases in theory (Figure 3c,d), which are well matched by the experimental samples containing the chiral switch and S1 or R1 with different concentrations (Tables S1 and S2, Supporting Information). Notably, for the conflict-depended binary chiral system, $w_1$ must be less than 40.14%, or else the variation of the HTP values exists no different with the cooperation-dependent binary chiral system. The predictable HTP values ensure the precise and reliable manipulation of photonic bands in the visible-light-actuated CLCs (Table S3, Supporting Information).

According to Bragg's law Equation (6) and the HTP measurement Equation (7), the reflection wavelength ($\lambda$) and the tuning range ($\Delta\lambda$) are derived below:

$$\lambda = n \cdot p \tag{6}$$

$$\beta = \frac{1}{p \cdot c} \tag{7}$$

$$\lambda_0 = \frac{n}{\beta_0 \cdot c} \tag{8}$$

$$\lambda_{PSS530} = \frac{n}{\beta_{PSS530} \cdot c} \tag{9}$$

$$\Delta\lambda = \lambda_{PSS530} - \lambda_0 = \frac{n}{c} \cdot \frac{-67w_1}{\beta_0 \cdot \beta_{PSS530}} \tag{10}$$

$$c = c_1 + c_2 \tag{11}$$

where $n$ is the average refraction index of the LC host E7 (n = 1.747), $p$ is the effective pitch length of the helix, $c$ is the additive molar concentration of both the chiral switch and the chiral dopant (S1 or R1), $\lambda_0$ and $\lambda_{PSS530}$ are reflection wavelengths at the initial state and the $PSS_{530}$, respectively. Since $\beta_0$ and $\beta_{PSS530}$ are decided by $w_1$, $\lambda_0$ and $\Delta\lambda$ are concluded to relate to two parameters of $w_1$ and $c$ from the equations above. When preset the certain $\lambda$ and $\Delta\lambda$, the corresponding solutions of $c_1$ and $c_2$ are decided. For example, to obtain the initial reflection wavelength of 600 nm with a tuning range of 50 nm in CLCs composed of chiral switch and S1(Sample 11 in Table S3, Supporting Information), the $w_1$ and $c$ are calculated as the unique solution of 6.5 (mol%) and 6.0 (mol%). Theoretically, any combination of $\lambda$ and $\Delta\lambda$ within the tuning range of HTP values is manipulable at suitable concentrations of chiral switches and dopants. For the light-driven CLCs containing one single chiral switch, only the initial reflection wavelength or the tuning range can be

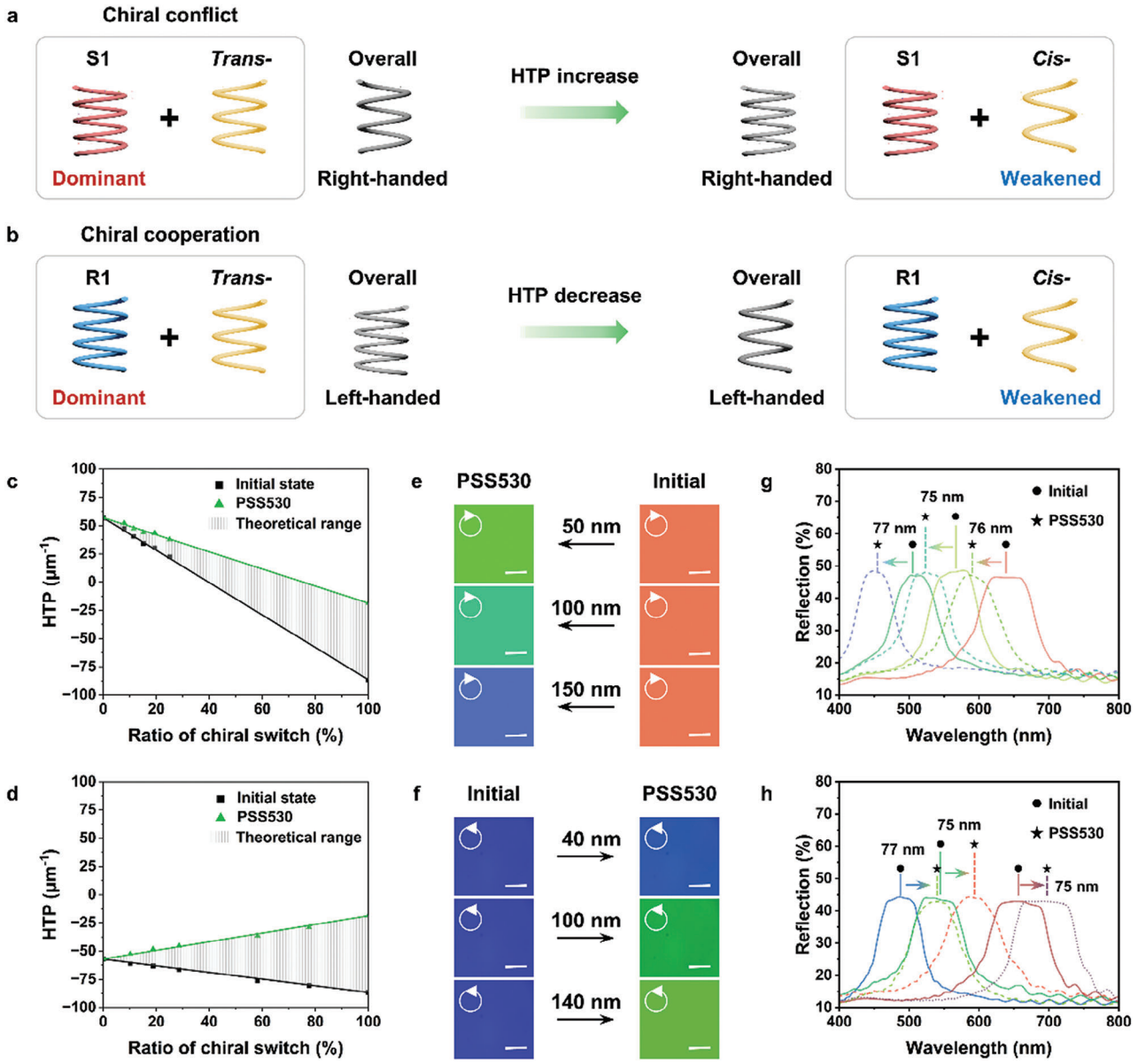


**Figure 3.** a) Schematic illustration to show the chiral conflict in a CLC doped with a binary chiral system containing a chiral switch and S1 that possesses opposite chirality. The overall right-handed helical superstructures wind due to the increase of the HTP value. b) Schematic illustration to show the chiral cooperation in a CLC doped with a binary chiral system containing a chiral switch and R1 that possesses the same chirality. The overall left-handed helical superstructures unwind due to the decrease of the HTP value. c,d) Plots to show the ratio of the chiral switch versus the HTP of the binary chiral system containing (c) S1 and (d) R1. (+) and (−) represent right-handed and left-handed helical twisting sense, respectively. Samples 1–10 were used to measure the HTP values (Table S1 and Table S2, Supporting Information). e,f) Polarized optical microscope images of the CLCs with different CPR in 5 μm thick planar aligned cells to show the (e) blueshift and (f) redshift of phototunable structural colors from the same initial state to the different $PSS_{530}$. Scale bar, 100 μm. g,h) Reflection spectra to show the equidistant phototuning range of the CLCs with different CPR from the initial state to the $PSS_{530}$ during (g) blueshift and (h) redshift. Samples 11–22 were used to test the dynamic phototuning range (Table S3, Supporting Information).

specified as desirable due to the one common relevant parameter of concentration. On the contrary, the binary chiral systems additionally introduce a variable to increase the flexibility of manipulation, therefore breaking the limitation of the restrictive relationship between the initial reflection wavelength and the tuning range and providing a platform for a versatile combination of chiral molecules to precisely manipulate the self-assembly helical superstructures.

Combining the above two features of optional shift direction and controllable tuning range, both left-handed and right-handed CPR are precisely manipulated in the systems arising from the chiral conflict and cooperation. Particularly, diverse tuning ranges with a certain initial reflection wavelength (Figure 3e,f; Figures S8 and S9, Supporting Information) can be realized, and vice versa (Figure 3g,h). First, the former was manipulated in the CLCs composed of binary chiral systems (visible-light-driven

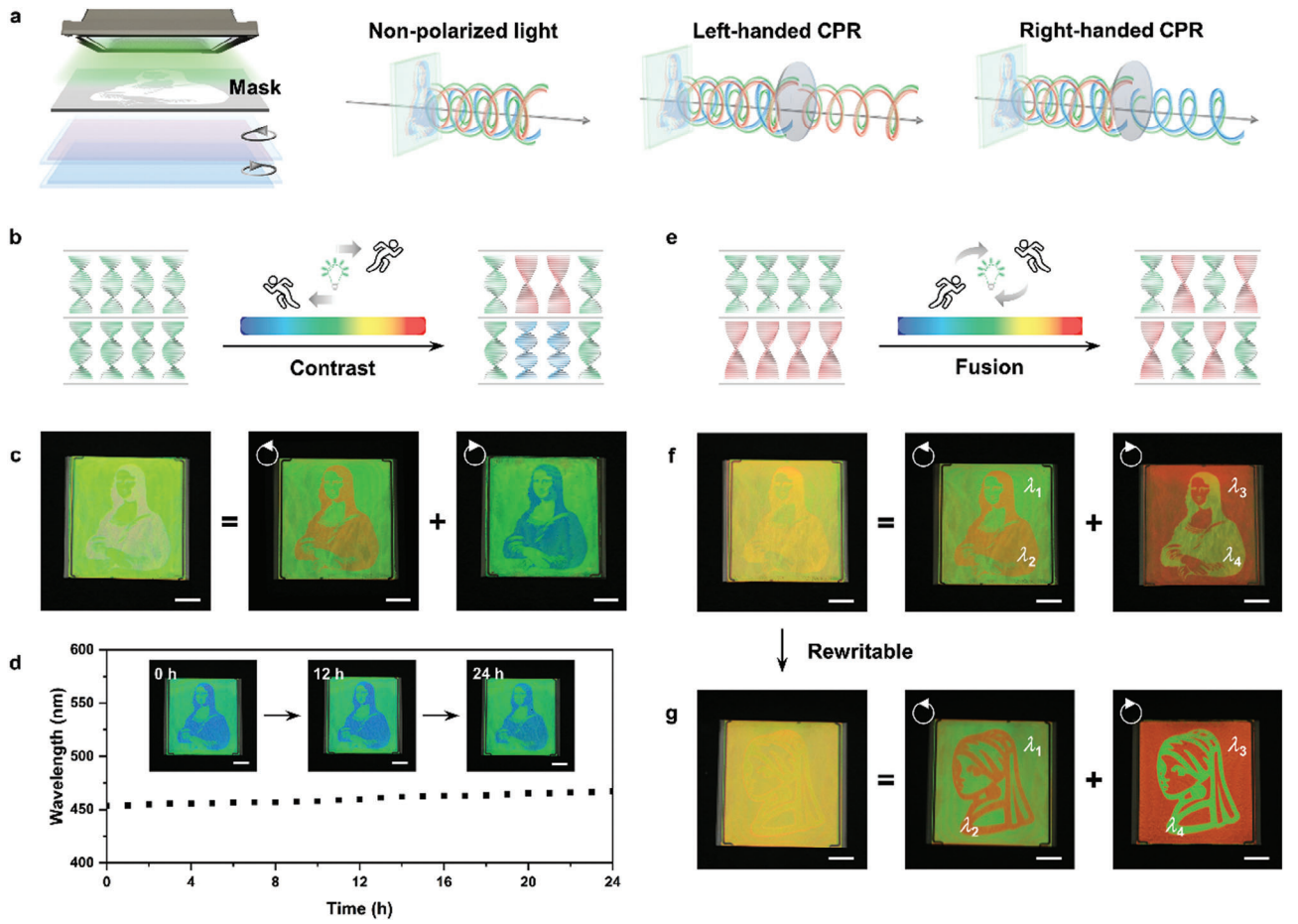


**Figure 4.** a) Schematic illustration to show the localized color tuning of the double-layer CLCs via a photomask upon exposure to 530 nm light, and the observation of the patterns with different CPR. The helical superstructures of the CLCs in the top and bottom layers are left-handed and right-handed, respectively. The double-layer CLCs show non-polarized reflection under natural light while showing left-handed CPR or right-handed CPR under a left-handed circular polarizer or right-handed circular polarizer, respectively. b) Schematic illustration to show the "contrast" mode for locally tuning pitch lengths in the double-layer CLCs. c) Photographs of the double-layer CLCs to show the photochromic pattern of the *Mona Lisa Smile*. The structural coloration under natural light (right) is the overlay of the left-handed (middle) and right-handed CPR (right). Scale bar, 1 cm. d) Dark thermal relaxation of the visible-light-actuated CLCs after 530 nm light irradiation to reach $PSS_{530}$. The reflection wavelength recovers from 453 to 467 nm in 24 h. Inset, time sequence photographs to show the structural coloration of the photochromic patterns at 0, 12, and 24 h. e) Schematic illustration to show the "fusion" mode for locally tuning pitch lengths in the double-layer CLCs. f) Photographs of the double-layer CLCs to show the photochromic pattern of the *Mona Lisa*, which is rewritable by 530 nm light after erasing by 445 nm light or thermal relaxation as g) the pattern of the *Girl with the Pearl Earring*. The structural coloration under natural light (right) is the overlay of the left-handed (middle) and right-handed CPR (right). ($\lambda_1$, $\lambda_3$) and ($\lambda_2$, $\lambda_4$) represent the reflection wavelengths at the initial state and $PSS_{530}$, respectively. Scale bar, 1 cm.

chiral switch and S1) based on chiral conflict. The initial red right-handed CPR ($\lambda \approx 610$ nm) was turned to show green (555 nm), cyan (510 nm), and blue (460 nm) at the $PSS_{530}$ with a tuning range of 50, 100, and 150 nm, respectively (Figure 3e; Figure S8, Supporting Information). Correspondingly, for the binary chiral system (the visible-light-driven chiral switch and R1) based on chiral cooperation, the initial blue left-handed CPR ($\lambda \approx 435$ nm) redshift with 40, 100, and 140 nm show blue (475 nm), green (535 nm), and chartreuse (575 nm) at the $PSS_{530}$, respectively (Figure 3f; Figure S9, Supporting Information). Alternatively, the latter that different initial reflection wavelengths with the equidistant tuning range at ≈75 nm were regulated in both CLC systems (Figure 3g,h; Figure S10, Supporting Information). These results manifest that our binary chiral systems based on chiral cooperation and conflict enable the achievement of tuning multiple optical DOFs, including circular polarization, shift direction of photochromism, and range of photonic bands. In this scenario, the visible-light-actuated CLCs were used to create patterns with desirable structural colors by using the photomasks with sports icons upon exposure to 530 nm light (Figure S10, Supporting Information). For example, the reflection wavelengths of the exposed areas were optionally tuned to show blue "badminton" (Sample 19) or red "taekwondo" (Sample 21) while the background remained the prescribed green color.

To gain further insight into the multi-DOF photoprogramming of the CLCs, we create patterns with dual light-driven photonic bandgaps to show various structural colors under different optical conditions (**Figure** 4a). The minimum pixel size of the patterns created via a photomask is ≈285 μm (Figure S11,

Supporting Information). The larger the size of the photomask, the more exquisite the edge of the patterns. Two layers of the CLCs induced by the binary chiral systems based on chiral cooperation (top layer) and conflict (bottom layer) were tightly overlapped. By using the photomask with a pattern of the *Mona Lisa*, the reflection wavelengths of double-layer CLCs simultaneously turn upon localized exposure to 530 nm light. The pattern demonstrates superimposed colors originating from the two layers under non-polarized light, while only the colors of the top layer are observed under left-handed circular polarization, or else the colors of the bottom layer are observed under right-handed circular polarization. Therefore, any two wavelength bands can be selected to provide structural colors that cannot be developed with a single band.[59]

Based on the precisely manipulable range of photonic bands and shift direction, two typical modes were realized for creating the patterns in the double-layer CLCs, including "contrast" and "fusion". In "contrast" mode, the initial reflection wavelength of the two layers is tuned exactly in coincidence but shifts to the opposite direction to show contrast structural colors at the $PSS_{530}$ after irradiation (Figure 4b,c). For example, by locally tuning the consistent pitch lengths in the double-layer CLC, green-to-red (top layer) and green-to-blue (bottom layer) transformations were induced at the same time. Therefore, in the absence of polarization, the created pattern of the *Mona Lisa Smile* displays magenta, which was analyzed into red under the left-handed circular polarization and blue under the right-handed circular polarization (Figure 4c). The variation of reflection wavelengths turning to the opposite direction greatly improves the contrast of the structural color as well as visibility.[60] Moreover, The reflection wavelength of the main pattern at $PSS_{530}$ remained without obvious shift after 24 h, suggesting acceptable fatigue resistance (Figure 4d), although the diffusion causes blur in the edge of the patterns observed by an optical microscope (Figure S12, Supporting Information). The dark relaxation was extremely slow thanks to the thermally stable *cis* isomer of the fluoroazobenzene photoswitches with a remarkably long half-life. Furthermore, the "fusion" mode strictly requires the precise manipulation of both the initial reflection wavelength and the tuning range. On the premise of an identically given tuning range, the structural colors of each layer at the initial state and $PSS_{530}$ exchange with the other, reaching a uniform visual appearance after superimposition (Figure 4e,f,g). For example, the initial green ($\lambda_1$) was designed to turn as red ($\lambda_2$) at $PSS_{530}$ in the top layer while the initial red ($\lambda_3$) shifted to green ($\lambda_4$) at $PSS_{530}$ in the bottom layer, especially since $\lambda_1$ was equal to $\lambda_4$ and $\lambda_2$ was equal to $\lambda_3$. In this way, the color mixed by the double layers was almost identical, so that the created patterns were concealed. As a proof of concept, we further realized multi-channel encryption in the double-layer CLCs (Figure 4f), which display uniform yellow without any pattern under natural light but appear distinguishable red *Mona Lisa Smile* pattern with a green background under the left-handed circular polarization and inverted color of both pattern and background under the right-handed circular polarization. The encrypted pattern can be rewritten as other patterns (such as the *Girl with the Pearl Earring*) by cyclic illumination of 530 and 445 nm light (Figure 4g; Figure S13, Supporting Information).

## 3. Conclusion

In summary, we proposed a new paradigm to precisely manipulate the self-assembly of helical superstructures in CLCs by utilizing visible-light-driven binary chiral systems. The interaction between the two kinds of chiral molecules based on cooperation or conflict dominates the overall helicity and variation of HTP, endowing CLCs with multiple optical DOFs, including circular polarization, the shift direction of photochromism, and the tuning range of photonic bands. Especially, any combination of initial reflection wavelength with a certain tuning range was satisfied in theory by adjusting the ratio of the components in binary chiral systems. The strategy enriches the choice of chiral systems and promotes a leap for manipulating structural colors from a qualitative to semiquantitative and even quantitative way, which has not been achieved in CLCs with a single responsive chiral molecule or other diverse photonic crystals. Taking advantage of the structural colors with optional CPR and controllably bidirectional photochromism, polarized reflection patterns concealed under non-polarized light are realized in a two-layer CLC film. The patterning concept provides a versatile platform for advanced applications of display, multiplexed communication, and information security.

## 4. Experimental Section

*Materials*: All chemical reagents were purchased from Adamas-beta and were used as supplied without further purification. The LC host E7 ($n$ = 1.747), standard chiral dopants S811 and R811 were purchased from Nanjing Murun Advanced Material Co., Ltd. Wedge cells (KCRK-07) were purchased from Beijing Bayi Space LCD Technology Co., Ltd. The antiparallel aligned cells (the size of the cells is $2.5 \times 2$ cm$^2$ or $5 \times 5$ cm$^2$, the spacer is 5 µm) were purchased from Jiya (Langfang) Electronics Co., Ltd. The preparation of the visible-light-driven chiral switch and the chiral dopants (R1 and S1), and the HTP measurement are described in the Supporting Information online.

*Preparation of the CLC Mixtures*: The visible-light-driven chiral switch, the chiral dopant (R1 or S1), and LC host E7 were mixed in dichloromethane solution to prepare the homogenous CLC mixtures after evaporation of the solvent. The obtained CLC mixtures were stored in the dark.

*Measurements*: $^1$H NMR, $^{13}$C NMR, and $^{19}$F NMR spectra were recorded on a Bruker AVANCE III spectrometer at 400 MHz with the use of $CDCl_3$ as the lock. Melting points were measured on a TA Q2000 differential scanning calorimeter. Mass spectra were recorded on an AB SCIEX 5800 mass spectrometer. UV–vis spectra of the QD inks were measured by using a UV–vis spectrometer (PerkinElmer Lambda 650, 200–800 nm) at a resolution of 2 nm. The textures and the disclination lines of the CLC mixtures were observed by using a polarized optical microscope (OPTEC BK-POL). Reflection spectra were recorded by using a reflection spectrometer (Ideaoptics Instruments PG2000-Pro-EX, 200–1100 nm). 365 nm UV light was generated by using a light source (Omron ZUV-H30MC) with a controller (ZUV-C30H). 530 nm green light was generated by using a light source (CCS HLV-24GR-3 W) with a controller (PJ-1505-2CA). 445 nm blue light was generated by using a light source (Jardon OE, JD BL-445-300). Photographs and videos were recorded using a digital camera (Canon EOS 70D).

## Supporting Information

Supporting Information is available from the Wiley Online Library or from the author.

## Acknowledgements

This work was financially supported by the National Natural Science Foundation of China (52173110), Natural the Science Foundation of Shanghai (21ZR1405900), and the Shanghai Rising-Star Program (22QA1401200).

## Conflict of Interest

The authors declare no conflict of interest.

## Data Availability Statement

The data that support the findings of this study are available from the corresponding author upon reasonable request.

## Keywords

anti-counterfeiting, chiral conflict, liquid crystals, photonic crystals, photoswitches

Received: August 13, 2024
Revised: September 26, 2024
Published online:

[1] P. Vukusic, *Science* **2009**, *325*, 398.
[2] V. V. Vogler-Neuling, M. Saba, I. Gunkel, J. O. Zoppe, U. Steiner, B. D. Wilts, A. Dodero, *Adv. Funct. Mater.* **2023**, 2306528.
[3] M. Mitov, *Adv. Mater.* **2012**, *24*, 6260.
[4] V. Sharma, M. Crne, J. O. Park, M. Srinivasarao, *Science* **2009**, *325*, 449.
[5] E. D. Finlayson, L. T. McDonald, P. Vukusic, *J. R. Soc. Interface* **2017**, *14*, 20170129.
[6] Y. Liu, P. Xing, *Adv. Mater.* **2023**, *35*, 2300968.
[7] X. Zhang, Y. Xu, C. Valenzuela, X. Zhang, L. Wang, W. Feng, Q. Li, *Light: Sci. Appl.* **2022**, *11*, 223.
[8] L. Wang, A. M. Urbas, Q. Li, *Adv. Mater.* **2020**, *32*, 1801335.
[9] Y. Zhang, Z. G. Zheng, Q. Li, *Responsive Mater.* **2024**, *2*, 20230029.
[10] D. Qu, H. Zheng, H. Jiang, Y. Xu, Z. Tang, *Adv. Optical Mater.* **2019**, *7*, 1801395.
[11] M. Zhang, Q. Guo, Z. Li, Y. Zhou, S. Zhao, Z. Tong, Y. Wang, G. Li, S. Jin, M. Zhu, T. Zhuang, S. H. Yu, *Sci. Adv.* **2023**, *9*, eadi9944.
[12] Y. Geng, R. Kizhakidathazhath, J. P. F. Lagerwall, *Nat. Mater.* **2022**, *21*, 1441.
[13] C. Yuan, J. Chen, B. Liu, P. Sun, H. Hu, Y. Tang, Y. Wang, Y. Zhan, M. Li, Z. Zheng, Q. Li, *Matter* **2023**, *6*, 3555.
[14] J. Ma, Y. Yang, C. Valenzuela, X. Zhang, L. Wang, W. Feng, *Angew. Chem., Int. Ed.* **2022**, *61*, 202116219.
[15] J. A. H. P. Sol, H. Sentjens, L. Yang, N. Grossiord, A. P. H. J. Schenning, M. G. Debije, *Adv. Mater.* **2021**, *33*, 2103309.
[16] R. Mujica, A. Augustine, M. Pauly, Y. Battie, G. Decher, V. L. Houérou, O. Felix, *Adv. Mater.* **2024**, *36*, 2401742.
[17] S.-U. Kim, Y.-J. Lee, J. Liu, D. S. Kim, H. Wang, S. Yang, *Nat. Mater.* **2021**, *21*, 41.
[18] X. Chen, H. K. Bisoyi, X.-F. Chen, X.-M. Chen, S. Zhang, Y. Tang, G. Zhu, H. Yang, Q. Li, *Matter* **2022**, *5*, 3883.
[19] D. Lou, Y. Sun, J. Li, Y. Zheng, Z. Zhou, J. Yang, C. Pan, Z. Zheng, X. Chen, W. Liu, *Angew. Chem., Int. Ed.* **2022**, *61*, 202117066.
[20] L. Qin, X. Liu, K. He, G. Yu, H. Yuan, M. Xu, F. Li, Y. Yu, *Nat. Commun.* **2021**, *12*, 699.
[21] X. Lai, Q. Ren, F. Vogelbacher, W. E. I. Sha, X. Hou, X. Yao, Y. Song, M. Li, *Adv. Mater.* **2021**, *34*, 2107243.
[22] K. E. Shopsowitz, H. Qi, W. Y. Hamad, M. J. Maclachlan, *Nature* **2010**, *468*, 422.
[23] K. R. Schlafmann, M. S. Alahmed, K. L. Lewis, T. J. White, *Adv. Funct. Mater.* **2023**, *33*, 2305818.
[24] S. I. Lim, E. Jang, D. Yu, J. Koo, D. G. Kang, K. M. Lee, N. P. Godman, M. E. McConney, D. Y. Kim, K. U. Jeong, *Adv. Mater.* **2022**, *35*, 2206764.
[25] X. Liu, L. Qin, Y. Yu, *Acta Phys.-Chim. Sin.* **2023**, *40*, 2305018.
[26] Y. Li, M. Wang, T. J. White, T. J. Bunning, Q. Li, *Angew. Chem., Int. Ed.* **2013**, *125*, 9093.
[27] S. J. Liu, L. Zhu, Y. H. Zhang, W. Chen, D. Zhu, P. Chen, Y. Q. Lu, *Adv. Mater.* **2023**, *35*, 2301714.
[28] X. Zhang, L. Li, Y. Chen, C. Valenzuela, Y. Liu, Y. Yang, Y. Feng, L. Wang, W. Feng, *Angew. Chem., Int. Ed.* **2024**, *63*, 202404202.
[29] X. Zhan, F. F. Xu, Z. Zhou, Y. Yan, J. Yao, Y. S. Zhao, *Adv. Mater.* **2021**, *33*, 2104418.
[30] A. J. J. Kragt, D. C. Hoekstra, S. Stallinga, D. J. Broer, A. P. H. J. Schenning, *Adv. Mater.* **2019**, *31*, 1903120.
[31] X. Wang, B. Zhao, J. Deng, *Adv. Mater.* **2023**, *35*, 2304405.
[32] H. Park, H. J. Lee, H. Ahn, W. C. Han, H. S. Yun, Y. S. Choi, D. S. Kim, D. K. Yoon, *Adv. Optical Mater.* **2024**, *12*, 2400266.
[33] L. L. Ma, C. Liu, S. B. Wu, P. Chen, Q. M. Chen, J. X. Qian, S. J. Ge, Y. H. Wu, W. Hu, Y. Q. Lu, *Sci. Adv.* **2021**, *7*, eabh3505.
[34] H. Hu, M. He, X. Liang, M. Li, C. Yuan, B. Liu, X. Liu, Z. G. Zheng, W. H. Zhu, *Matter* **2023**, *6*, 3927.
[35] R. Lan, J. Bao, Z. Li, Z. Wang, C. Song, C. Shen, R. Huang, J. Sun, Q. Wang, L. Zhang, H. Yang, *Angew. Chem., Int. Ed.* **2022**, *61*, 202213915.
[36] R. Zheng, Y. Wei, Z. C. Zhang, Z. Y. Wang, L. L. Ma, Y. Wang, L. Huang, Y. Q. Lu, *Responsive Mater.* **2023**, *1*, 20230017.
[37] H. K. Bisoyi, Q. Li, *Chem. Rev.* **2016**, *116*, 15089.
[38] H. K. Bisoyi, Q. Li, *Angew. Chem., Int. Ed.* **2016**, *55*, 2994.
[39] P. Chen, L. L. Ma, W. Hu, Z. X. Shen, H. K. Bisoyi, S. B. Wu, S. J. Ge, Q. Li, Y. Q. Lu, *Nat. Commun.* **2019**, *10*, 2518.
[40] J. Liu, J. J. Wu, J. Wei, Z. J. Huang, X. Y. Zhou, J. Y. Bao, R. C. Lan, Y. Ma, B. X. Li, H. Yang, Y. Q. Lu, Q. Zhao, *Angew. Chem., Int. Ed.* **2024**, *63*, 202319536.
[41] J. Lv, D. Ding, X. Yang, K. Hou, X. Miao, D. Wang, B. Kou, L. Huang, Z. Tang, *Angew. Chem., Int. Ed.* **2019**, *58*, 7783.
[42] S. Lin, K. G. Gutierrez-Cuevas, X. Zhang, J. Guo, Q. Li, *Adv. Funct. Mater.* **2020**, *31*, 2007957.
[43] S. Zhang, Y. An, X. m. Chen, Q. Li, *Smart Mol.* **2023**, *1*, 20230015.
[44] L. Qin, J. Wei, Y. Yu, *Adv. Optical Mater.* **2019**, *7*, 1900430.
[45] S. Cui, L. Qin, X. Liu, Y. Yu, *Adv. Optical Mater.* **2022**, *10*, 2102108.
[46] Y. Li, C. Xue, M. Wang, A. Urbas, Q. Li, *Angew. Chem., Int. Ed.* **2013**, *52*, 13703.
[47] H. Hayasaka, T. Miyashita, M. Nakayama, K. Kuwada, K. Akagi, *J. Am. Chem. Soc.* **2012**, *134*, 3758.
[48] Z. G. Zheng, Y. Li, H. K. Bisoyi, L. Wang, T. J. Bunning, Q. Li, *Nature* **2016**, *531*, 352.
[49] A. Ryabchun, F. Lancia, J. Chen, D. Morozov, B. L. Feringa, N. Katsonis, *Adv. Mater.* **2020**, *32*, 2004420.
[50] R. A. van Delden, N. Koumura, N. Harada, B. L. Feringa, *Proc. Natl. Acad. Sci. U.S.A.* **2002**, *99*, 4945.
[51] K. Kumar, C. Knie, D. Bleger, M. A. Peletier, H. Friedrich, S. Hecht, D. J. Broer, M. G. Debije, A. P. Schenning, *Nat. Commun.* **2016**, *7*, 11975.
[52] H. Wang, H. K. Bisoyi, A. M. Urbas, T. J. Bunning, Q. Li, *J. Am. Chem. Soc.* **2019**, *141*, 8078.
[53] S. Iamsaard, E. Anger, S. J. Aβhoff, A. Depauw, S. P. Fletcher, N. Katsonis, *Angew. Chem., Int. Ed.* **2016**, *55*, 9908.
[54] M. J. Hansen, M. M. Lerch, W. Szymanski, B. L. Feringa, *Angew. Chem., Int. Ed.* **2016**, *128*, 13712.
[55] L. Qin, W. Gu, J. Wei, Y. Yu, *Adv. Mater.* **2018**, *30*, 1704941.

[56] Z. G. Zheng, Y. Q. Lu, Q. Li, *Adv. Mater.* **2020**, *32*, 1905318.
[57] D. Bleger, J. Schwarz, A. M. Brouwer, S. Hecht, *J. Am. Chem. Soc.* **2012**, *134*, 20597.
[58] I. Dierking, *Textures of Liquid Crystals*, VCH, Weinheim, **2003** pp. 66.
[59] S. S. Lee, H. J. Seo, Y. H. Kim, S. H. Kim, *Adv. Mater.* **2017**, *29*, 1606894.
[60] L. Jia, M. Li, L. Jiang, H. Gao, H. Tan, B. Peng, J. Xu, L. Zhang, J. Zhu, *J. Mater. Chem. C* **2020**, *8*, 9286.